PCCP

PAPER

View Article Online
View Journal | View Issue

Cite this: *Phys. Chem. Chem. Phys.*, 2025, **27**, 11649

The role of branching in the ultrafast dynamics and two-photon absorption of two pyrimidine push–pull molecules†

Alexandros Katsidas,[a] Michaela Fecková,[bcd] Filip Bureš,[cd] Sylvain Achelle[b] and Mihalis Fakis*[a]

The dynamics and two-photon absorption (2PA) properties of two pyrimidine chromophores are studied using femtosecond time-resolved fluorescence and two-photon excited fluorescence techniques. The pyrimidine is used as an electron withdrawing group and is substituted at the C2 position with a phenylacridan fragment, while diphenylaministyryl donor moieties are appended at positions C4/6 to afford the pseudo-dipolar and pseudo-quadrupolar molecules **1** and **2**, respectively. Chromophore **2** shows more efficient fluorescence emission, while **1** exhibits larger Stokes shifts. Their decay pathways are discussed through an emission from a Franck–Condon charge transfer (FC-CT) and a relaxed charge transfer (R-CT) state. Ultrafast dynamics in tetrahydrofuran show population of the R-CT state for **1** that is faster than solvation, while for **2**, due to its pseudo-quadrupolar nature, R-CT population is slower and occurs from the solvated FC-CT state. Finally, molecule **2** shows better 2PA properties with cross sections reaching 560 GM at 820 nm.

Received 13th February 2025,
Accepted 6th May 2025

DOI: 10.1039/d5cp00589b

rsc.li/pccp

Introduction

Intramolecular charge transfer (ICT) in push–pull π-conjugated organic chromophores is a fundamental process, controlling the nature and dynamics of the excited states, the photophysical properties and the potential for future applications of these chromophores in diverse and emerging photonic applications.[1–6] It also plays a crucial role in various biophysical phenomena.[7–10] The population of ICT states occurs in chromophores of dipolar, quadrupolar and octupolar topology and depends not only on the electron donating/withdrawing groups and the π-conjugated core but also on the molecular environment. In solution, the polarity of the solvent affects the energy level of the ICT state, rendering its population energetically favorable.[11–16] Emission by an ICT state is characterized by a low-energy, broad and structureless emission spectrum with a reduced fluorescence quantum yield (Φ), compared to the narrow and vibronically structured emission stemming from a Franck–Condon (FC) state.[17–20] Often, the ICT process leads to the population of a number of states with variable degrees of charge-transfer (CT) or to an excited state conformation with a twisted morphology (TICT), resulting in a very broad spectrum with dual peaks.[21–27]

The ICT takes place within the excited state lifetime and especially in the timescale of 100 fs to a few ps. It often occurs simultaneously with solvent relaxation, structural reorganization and isomerization, leading to rich and complicated photodynamics. Separating the above kinetic phenomena is typically a non-trivial task.[28–30] In dipolar (D–π–A) molecules, ICT is typically expected and is easily manifested by significant positive emission solvatochromism. In quadrupolar and octupolar molecules, ICT is related to the excited state symmetry breaking (SB), a phenomenon that has attracted significant scientific interest.[31–37] SB is decisively dependent on solute–solvent interactions since the solvent's strong reaction field enhances SB and an excited state of quadrupolar nature relaxes to a dipolar state.

Molecules with ICT properties have been the subject of intense scientific interest since a deep understanding of the control and modulation of ICT is imperative for advances in photonic devices. They have demonstrated enhanced electro-optic coefficients,[38,39] second harmonic generation efficiency[40,41] and two-photon absorption (2PA) properties.[17,42–50] Especially, due to their non-linear optical (NLO) properties, they are attractive for a variety of applications in imaging,[51] photodynamic therapy,[52] optical limiting,[53,54] direct laser microfabrication and 3D optical

[a] Department of Physics, University of Patras, Patras, 26504, Greece. E-mail: fakis@upatras.gr; Tel: +30 2610 996794
[b] Univ Rennes, CNRS, ISCR (Institut des Sciences Chimiques de Rennes)-UMR 6226, F-35000, Rennes, France
[c] Institute of Organic Chemistry and Technology, Faculty of Chemical Technology, University of Pardubice, Studentská 573, Pardubice, 53210, Czechia
[d] Institute of Technology and Business in České Budějovice, Okružní 517/10, České Budějovice, 37001, Czechia

† Electronic supplementary information (ESI) available. See DOI: https://doi.org/10.1039/d5cp00589b

data storage.[55–57] Moreover, they have also exhibited reverse intersystem crossing (RISC) and excellent thermally activated delayed fluorescence (TADF) properties due to a small energy gap between singlet and triplet excited states.[58–61] Finally, aggregation induced emission (AIE) has also been reported for push–pull structures,[62,63] rendering these ICT molecules highly suitable for next-generation organic light emitting diodes (OLEDs), while they are also finding use in organic solar cells as electron acceptors.[64,65]

As it is easily understood, push–pull molecules with ICT properties are appealing not only from a fundamental point of view but also due to a plethora of applications. Alkyl-amino, phenyl-amino, 9*H*-carbazol-9-yl and acridan fragments are some of the most well-known groups to be used as electron donors.[66–71] On the other hand, various heterocyclic rings have been investigated as electron withdrawing groups in ICT molecules such as benzothiazole and triazine.[72–75] The pyrimidine group with two nitrogen atoms has been used as a suitable fragment in NLO chromophores, in TADF emitters and in stimuli responsive fluorescence switches.[76–79] In our recent work, we have reported on the synthesis of six 4-styryl or 4,6-distyryl substituted pyrimidines linked to acridan at the C2 position *via* a phenylene linker. We have focused on their dual emission properties and long-lived ICT states.[80]

As a continuation of our previous work, we focus herein on the ultrafast dynamics and NLO properties of two previously reported pyrimidines, having diphenylamino donors connected to the styryl fragments. Ultrafast dynamics reveal emission by an initially excited Franck–Condon CT (FC-CT) state and a relaxed CT (R-CT) state due to solvent or structural reorganization, while good 2PA values are found. Based on ultrafast dynamics and 2PA measurements, it is concluded that the acridan group does not play a role in the emission process as it lies almost perpendicular to the adjacent phenyl ring.

Experimental

Steady state spectroscopy

The two molecules were examined for their steady state spectra in hexane (HEX), decane (DEC), toluene (TOL), tetrahydrofuran (THF), dichloromethane (DCM), acetone (ACT) and acetonitrile (MeCN). The absorption spectra were recorded with a Shimadzu UV-3000 spectrometer, while a Horiba S2 Jobin Yvon Fluoromax 4 was used for recording the steady-state fluorescence spectra. The Φ values were determined relative to that of 9,10-bis(phenylethynyl)anthracene in cyclohexane (Φ = 1.00).[81]

Time resolved spectroscopy

The time resolved fluorescence dynamics were studied in the ps–ns and fs–ps timescales by means of the time correlated single photon counting (TCSPC) and the femtosecond upconversion methods.[32,82] In the former, a ps diode laser at 400 nm, with a 60 ps pulse duration, was used as the excitation source. The detection was made under magic angle conditions for the determination of the lifetimes, while anisotropy measurements were also conducted to determine the rotational times. The overall temporal resolution of the technique was 80 ps. For the upconversion measurements, a fs mode-locked Ti:sapphire laser with 80 fs pulses was used. The second harmonic beam at 400 nm served as the excitation beam. The temporal resolution of the system was 250 fs. Again, both magic angle and anisotropy measurements were made. For the latter, the polarization plane of the excitation laser was changed using a Berek compensator. In both techniques, the time resolved anisotropy was calculated using

$$r(t) = \frac{I_{\mathrm{par}}(t) - I_{\mathrm{per}}(t)}{I_{\mathrm{par}}(t) + 2I_{\mathrm{per}}(t)}$$

where $I_{\mathrm{par}}(t)$ and $I_{\mathrm{per}}(t)$ are the fluorescence intensities with parallel and perpendicular polarizations to the excitation source's polarization plane. For the TCSPC, a correction factor, G, was determined to compensate for the different responses of the monochromator at the two perpendicular polarizations. For the upconversion technique, this factor is unity.

2PA spectroscopy

All the samples were fluorescent chromophores, so their 2PA properties were examined by a two-photon excited fluorescence (2PEF) technique from 730 to 870 nm using the same mode-locked Ti:sapphire fs laser mentioned above.[83–85] The 2PA fluorescence intensity was detected as a function of the excitation power, which was changed using a half-wave plate and a polarizer, always validating the square-law dependence. From these measurements, the 2PA cross sections ($\delta_{2\mathrm{PA}}$) were calculated using rhodamine 6G in MeOH (2×10^{-5} M) as the reference sample. The measured scattered light from the solvent has been subtracted.

Results and discussion

Materials

Fig. 1 shows the chemical structures of the two push–pull molecules **1** and **2** studied herein, both bearing a pyrimidine-based electron-acceptor central core. The pyrimidine is substituted at position C2 with a phenylacridan group. Also, diphenylamino substituted styryl moieties are appended in positions C4/6. The synthesis, using cross-coupling and Knoevenagel reactions, has been described previously, together with thermal properties, X-ray analysis and DFT-calculated

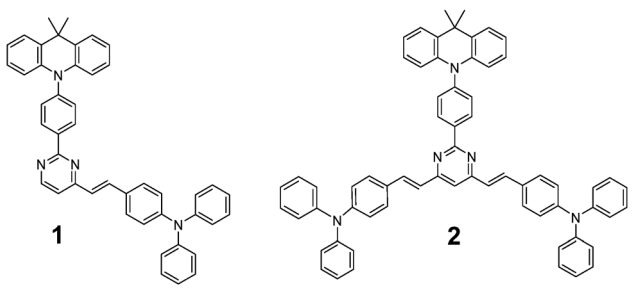

Fig. 1 The chemical structures of the pyrimidine-based molecules **1** and **2**.

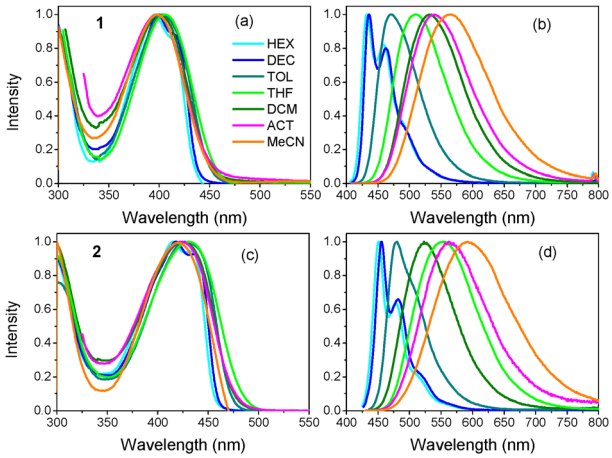

Fig. 2 Absorption (a) and (c) and emission (b) and (d) spectra of molecules **1** and **2** in various solvents.

parameters.[80] It was revealed that the acridan moiety has a perpendicular arrangement with respect to the residual π-system. Besides, non-zero ground state dipole moment was found while the compounds possess no symmetry.

Steady state spectroscopy

The fundamental optical properties of chromophores **1** and **2** were recorded in solutions with solvents of different polarity. Fig. 2 shows the absorption and emission spectra of the two molecules. Table 1 summarizes the photophysical results. The absorption spectra show a main peak at 400–430 nm attributed to the HOMO−1 to LUMO transition and account for an ICT transition.[80] In the apolar solvents HEX and DEC, both molecules feature slightly narrower and structured absorption spectra, while the structure is lost as the polarity increases. The shift of the spectra is however minimal pointing to an insignificant stabilization of the ground state.[86] The broadening, however, can be attributed to a ground state with a small degree of ICT nature.[18] The observed absorption solvatochromism is small and does not correlate with the orientational polarisability of the solvent.[87] It rather correlates with the refractive index, pointing to dispersion as the main solute–solvent interaction in the ground state. For **2**, the absorption spectra are red-shifted compared to **1** (by about 0.216 eV), which is typical for molecules with longer conjugation lengths, indicating an electronic coupling between the branches at positions C4 and C6. Such an electronic coupling is typical for branched compounds with a nitrogen atom as a central core, while it is hindered in the case of a benzene core due to a suppression of coherent interactions among the branches.[88–90]

As a quantitative investigation, the absorption transition dipole moments for **1** and **2** were calculated using the equation:[91]

$$\mu_{GE} = 9.854 \times 10^{-2}\left[\frac{1}{n}\frac{1}{[f(n)]^2}\int_{S1}\frac{\varepsilon(\nu)}{\nu}d\nu\right]^{1/2}$$

where n is the refractive index of the solvent, $f(n) = (n^2 + 2)/3n$, and $\varepsilon(\nu)$ is the molar absorption coefficient. The results of these calculations are presented in Table S1 (ESI†). μ_{GE}, in the various solvents, ranges from 5.93 to 7.60 D for **1** and from 10.29 to 11.03 D for **2**, following the differences in the molar absorption coefficient. For **2**, μ_{GE} is higher than that of **1**, as expected for a molecule with an increased conjugation length.

The emission spectra are more sensitive to solvent polarity as shown in Fig. 2. In apolar solvents, both molecules feature structured and narrow spectra with clear vibronic peaks attributed to a FC-CT state. Although only a qualitative comparison of the absorption and emission spectra can be made (a quantitative comparison involves plotting the spectra in cm^{-1}),[92] it is obvious that the mirror image rule is far from being obeyed in apolar solvents and this is due to an emission originating from a planar rigid structure due to an increase in the torsional barrier in the excited state.[93,94] On the other hand, in the ground state, the barrier is decreased, leading to an absorption from a variety of torsional arrangements. As the polarity increases, the spectra become broader, structureless and the peak is shifted to longer wavelengths, revealing the population of a R-CT state, which becomes the emitting state in polar environments. Finally, the fluorescence Φ values were measured for four representative solvents and were found to be significantly higher for **2** *vs.* **1**, reaching 0.94 in DCM.

Table 1 Optical properties of molecules 1 and 2

Molecule	Solvent	λ_{abs} (nm)/ε (mM^{-1} cm^{-1})	λ_{em} (nm)	Φ	Stokes shift (cm^{-1})	τ (ns)[a]	δ_{2PA} (GM)
1	HEX	396/24.4	432, 459	0.23	2100	0.87	150
	DEC	399	436, 463	—	2130	1.07	
	TOL	404/26.1	471	0.35	3520	1.44	110
	THF	400/34.0	508	0.47	5310	2.42	130
	DCM	406/31.3	532	0.75	5830	2.80	
	ACT	397	540	—	6670	2.96	
	MeCN	398	566	—	7460	2.91	
2	HEX	415, 433/65.1	451, 479	0.52	1920	1.25	560
	DEC	417, 436	456, 482	—	2050	1.36	
	TOL	426/62.1	480	0.65	2640	1.53	460
	THF	424/65.6	523	0.61	4460	2.38	460
	DCM	430/58.0	553	0.94	5170	2.89	
	ACT	422	563	—	5930	2.49	
	MeCN	419	592	—	6970	1.84	

[a] Taken as the average of the lifetimes measured by the TCSPC technique.

To obtain a deeper insight into the effect of polarity on the steady state spectra, the Lippert–Mataga plots were constructed, *i.e.* the Stokes shift was plotted as a function of solvent polarizability (Fig. S1, ESI†). As can be seen, molecule **2** has a slightly smaller Stokes shift for all the solvents and also a slightly smaller slope of the Lippert–Mataga plot. From the slope of these plots, the change of the permanent dipole moments $\Delta\mu_{solv}$ upon excitation can be calculated using the following equation:[18,95,96]

$$\nu_A - \nu_F = \frac{2(\mu_E - \mu_G)^2}{hca^3}\Delta f + \text{constant}$$

where h is Planck's constant, a is the Onsager cavity radius and $\mu_E - \mu_G$ is the change of the dipole moments $\Delta\mu_{solv}$. The solvent's polarizability is given by the equation:

$$\Delta f = f(\varepsilon) - f(n^2) = \frac{\varepsilon - 1}{2\varepsilon + 1} - \frac{n^2 - 1}{2n^2 + 1}$$

where ε is the dielectric constant and n is the refractive index of the solvent. Table S2 (ESI†) summarizes these values for all solvents. For the pseudo-dipolar chromophore **1**, the Onsager radius was estimated from its DFT-optimized structure as half of the distance between the Ph_2N donor occupied by the HOMO–1 and the LUMO spread over the central pyrimidine acceptor. For the pseudo-quadrupolar molecule **2**, the longest distance for the charge separation corresponds to the Ph_2N-centered HOMO–1 and the opposite olefinic linker bearing the LUMO (Fig. S2, ESI†).[97] Finally, $\Delta\mu_{solv}$ was found to be 9.85 D for **1** and 17.47 D for **2**, respectively (Table S3, ESI†).

Excited state dynamics

Fluorescence dynamics in the nanosecond timescale. To further investigate the mechanisms that occur after excitation, we performed TCSPC measurements, thus determining the excited states' lifetimes. The experimental results and fitting parameters are shown in Fig. 3 and Table S4 (ESI†), respectively. For both molecules, the fluorescence lifetime is in the range of ns and increases as the polarity is increased from the apolar HEX to medium-polarity DCM, owing to the stabilization of the ICT state, *e.g.* for **2**, the lifetime is 1.25 ns in HEX and 3.27 ns in DCM. In the most polar solvents ACT and MeCN, the lifetime decreases compared to the medium-polarity ones, revealing that as the ICT state is shifted to lower energies, nonradiative pathways become significant. However, this lifetime decrease is not very important compared to other push–pull molecules where a more than one order of magnitude decrease is observed.[34,82] The decay curves of molecule **2** are fitted with a single exponential function in low polarity solvents, while a two-exponential one is needed as the polarity increases. Based on these findings and the steady state spectra, τ_1 can be attributed to the lifetime of the FC-CT state, while τ_2 to the R-CT state. For **1**, the discussion of the lifetimes is similar, excluding the two apolar solvents HEX and DEC wherein a short lifetime of ~0.70 ns is observed, whose amplitude however reduces significantly in the latter solvent. This can be tentatively attributed to an unrelaxed excited state, which then relaxes to form a FC-CT state with a lifetime of 1.0–1.87 ns. Using the Φ values for HEX, TOL, THF and DCM and the average lifetimes, the radiative (k_{rad}) and non-radiative (k_{nrad}) decay rates were calculated (Table S5, ESI†). k_{rad} was in all cases higher for **2** ranging from 0.26 to 0.42 $\times$ 10^9 s^{-1}.

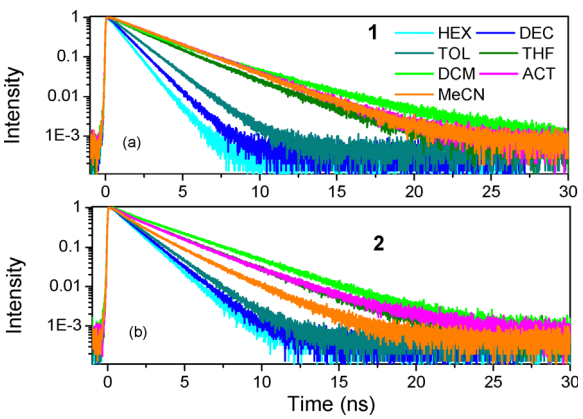

Fig. 3 Fluorescence decays in the nanosecond timescale for **1** and **2** in various solvents. Exc.: 400 nm, detection at the peaks of the emission spectra.

Next, the emission transition dipole moment is calculated using the lifetimes obtained by the TCSPC method and the following equation:[91]

$$\mu_{EG} = 1785.7\left[\frac{\Phi}{\tau n^3}\frac{1}{[f(n)]^2}\frac{1}{\tilde{\nu}_f^3}\right]^{1/2}$$

where Φ is the fluorescence quantum yield, τ is the average excited state lifetime, n is the solvent's refractive index, $f(n) = 3n/(2n^2 + 1)$ and $\tilde{\nu}_f^3$ is the average cubic fluorescence frequency expressed by:

$$\tilde{\nu}_f^3 = \frac{\int I(\nu)\mathrm{d}\nu}{\int I(\nu)/\nu^3\mathrm{d}\nu}$$

μ_{EG} can also provide useful information on the nature of the excited state. The values are summarized in Table S1 (ESI†) and are higher for **2** (*e.g.* μ_{EG} for **2** in DCM is 9.53 *vs.* 8.26 D for **1**) following the changes in the quantum yields.

Fluorescence dynamics in the femtosecond–picosecond timescale. The above-described fluorescence dynamics in the nanosecond timescale provided information on the decay pathways of the molecules. To gain a deeper insight into the time evolution of the systems' excited states, fluorescence upconversion measurements were carried out and the dynamics were examined within the first 130 ps in TOL and THF solutions. Due to the wavelength dependent nature of the dynamics in this short timescale, various measurements at different emission wavelengths were detected.

The dynamics along with the time-resolved emission spectra (TRES) and time-resolved area normalized emission spectra (TRANES) for TOL and THF are shown in Fig. 4 and 5 for **1** and **2**, respectively.[98–102] The 2D plots of the TRES are shown in Fig. S3 (ESI†). In all samples, a fast decay is observed at shorter

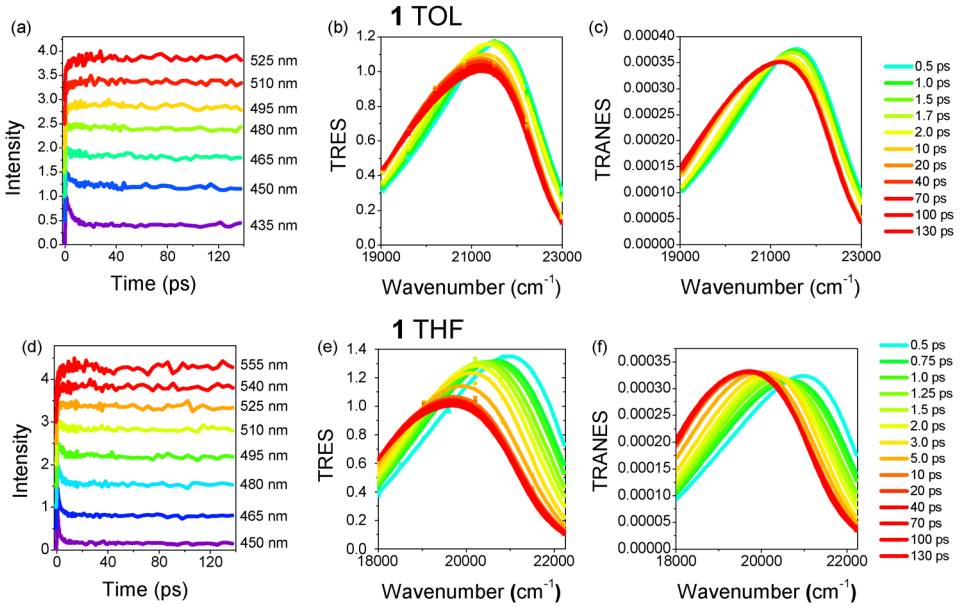

Fig. 4 (a) and (d) Fluorescence dynamics at selected wavelengths, (b) and (e) TRES and (c) and (f) TRANES for **1** in TOL and THF.

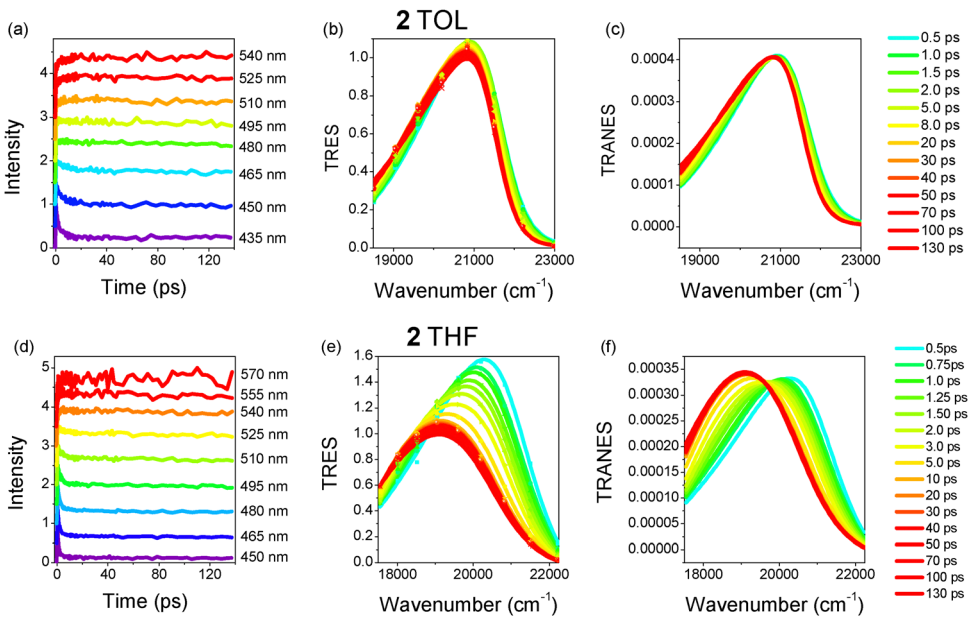

Fig. 5 (a) and (d) Fluorescence dynamics at selected wavelengths, (b) and (e) TRES and (c) and (f) TRANES for **2** in TOL and THF.

wavelengths and a slow rise at longer ones. This effect is due to a relaxation of the excited state towards lower energies caused by solvent/structural relaxation and R-CT population and leads to a red-shift of the emission spectrum. The curves were analyzed using a global fit method and the fitting results for the two faster mechanisms are shown in Tables S6 and S7 (ESI†). In all cases, a three-exponential fitting was needed to fit the results. The third (slowest) component was fixed to be equal to the lifetime found by the TCSPC technique. Within the ps timescale, two decay lifetimes of the order of ~1.3 ps and 5.9–6.6 ps in TOL and 0.6–0.8 and 2.5–2.8 ps in THF were found. The lifetimes correspond to decay mechanisms at short wavelengths (positive amplitudes), while they evolve to rise mechanisms (negative amplitudes) at longer ones. The relaxation times are smaller in THF for both molecules because it is a more polar solvent than TOL and the solute–solvent interactions are stronger. In both solvents, the relaxation times are similar to the solvation times for TOL and THF.[103,104]

The TRES of **1** in TOL exhibit a small transient red-shift (374 cm^{-1}), which is completed within ~10 ps, while the TRES of **2** remain almost unchanged with only a slight broadening. On the other hand, in THF the spectral changes are more obvious

with the spectra of both molecules having a significant red-shift (1313 cm^{-1} and 1171 cm^{-1} for **1** and **2**, respectively) within 10 ps. The solvent response function $C(t)$ for both molecules and solvents is plotted in Fig. S4 (ESI†). $C(t)$ decays faster in THF pointing to a more efficient spectral relaxation. A bi-exponential function was used to fit $C(t)$ with lifetimes similar to those found after global analysis of the individual dynamics pointing to inertial and diffusive solvation mechanisms (Table S8, ESI†). The total area-normalized intensity obtained by the TRES is also plotted in Fig. S4 (ESI†) and its dynamics is visually compared to the $C(t)$. In toluene, the total intensity exhibits a rise up to 2 ps, possibly due to vibronic relaxation. It is obvious that spectral relaxation *i.e* $C(t)$ is faster than quenching (intensity decrease) in toluene, while in the more polar THF, the spectral relaxation is highly related to the quenching of the excited state. Apart from the transient red-shift, the spectra are also accompanied by a gradual broadening, indicating a decay process involving more than one emitting state.[17,29] Fig. S5 (ESI†) shows the FWHM of the TRES as a function of time. Especially in the case of THF, for both compounds, an initial decrease of the FWHM is observed. This is due to a fast decay of the high energy rotamers to a rigid excited state.

Finally, following the method described by Vauthey *et al.*[105] and used by Xia *et al.*,[106] the instantaneous emission dipole moment, $\mu_{EG}(t)$, is calculated at different times for **1** and **2** in THF. The time dependence of $\mu_{EG}(t)$ is shown in Fig. S6 (ESI†) in non-normalized and normalized units. For both molecules, $\mu_{EG}(t)$ decreases within the first 10 ps reaching a constant value at longer times, which is equal to the emission dipole moment of the relaxed excited state as shown in Table S1 (ESI†). The decrease of $\mu_{EG}(t)$ is associated with a change in the nature of the excited state. The initial $\mu_{EG}(t)$ values of 9.5 and 7.5 D found for **1** and **2**, respectively, are considered as the emission dipole moments of the FC-CT state. The more intense decay of $\mu_{EG}(t)$ for **2** points to a change of its excited state from FC-CT with a pseudo-quadrupolar nature to an excited state with a stronger CT character.

Although the TRES provide a quantitative view of the spectral changes, further insight into the photodynamic mechanisms is obtained by observing the TRANES (Fig. 4 and 5). In TOL, both molecules have an iso-emissive point, indicating that there are two emissive species/states. The transient spectral changes for **1**, as mentioned above, are stronger than those of **2**, which could be ascribed to its dipolar nature, also revealed by the time resolved anisotropy and 2PA measurements (*vide infra*). The two emissive species could be considered as the FC-CT and R-CT states, while the contribution of the latter is less significant in the case of **2**. On the other hand, the two molecules reveal different and more pronounced behaviors in THF. **1** exhibits an iso-emissive point within the first 2 ps, while a gradual red-shift of the spectrum occurs at longer times and the iso-emissive point is lost (Fig. S7, ESI†). The iso-emissive point at short timescales is due to an emission from FC-CT and R-CT states with peaks at 21 000 cm^{-1} and 20 220 cm^{-1}, the latter being populated on a ~100 fs timescale, *i.e.* within the inertial solvation time for THF. Then, the emission from the R-CT state dominates and it relaxes at longer times (2–10 ps), leading to the observed transient red-shift to 19 700 cm^{-1}. Molecule **2** in THF shows exactly the opposite behavior. Initially, the spectrum experiences a transient shift in <3 ps (without an isosbestic point) due to an inertial and diffusion relaxation of the FC-CT state by the solvent molecules from 20 300 cm^{-1} to 19 500 cm^{-1} (Fig. S8, ESI†). After 3 ps, an iso-emissive point is revealed, which is an indication of the population of a R-CT state (at 19 100 cm^{-1}) by energy transfer from the FC-CT state and the simultaneous emission of both states. Fig. S9 (ESI†) shows an energy diagram that is used as a model for the explanation of the dynamics for **1** and **2** in THF. The population of the R-CT state for **2** occurs after solvation and is slower than for **1**, while the R-CT population for **1** is within the inertial solvent relaxation. This is attributed to the quadrupolar nature of **2** compared to the dipolar character of **1**.

Anisotropy dynamics

In our previous work, DFT analysis in molecules **1** and **2** revealed that the acridan moiety is rotated and lies off plane with respect to the pyrimidine core; therefore, it is not expected to play a crucial role in the optical properties and ICT process. To confirm this assumption, anisotropy measurements in the fs–ps timescale were conducted and the plots are shown in Fig. 6.

The initial anisotropy r_0 provides an aspect of the molecular symmetry after excitation. For dipolar molecules, r_0 is expected to be close to 0.4, while for quadrupolar and octupolar ones it is expected to be close to 0.2 and 0.1, respectively. For **1** and **2**, r_0 is 0.35 and 0.24–0.27, *i.e.* close to the values expected for dipolar (D–π–A) and quadrupolar (D–π–A–π–D) symmetry.[107–109] Also, no decay of the anisotropy in the 100 fs to ps timescale was observed for **2**, as expected for octupolar molecules due to coherent and incoherent energy delocalization mechanisms among the branches. Anisotropy decay measurements in the ns timescale were also performed to determine the rotational correlation time τ_{cor} as a function of solvent viscosity. τ_{cor} ranges from 0.15 ns to 0.38 ns for **1** and from 0.25 to 0.67 for **2** and is linearly dependent on the solvent viscosity (Fig. S10 and S11 and Table S9, ESI†).

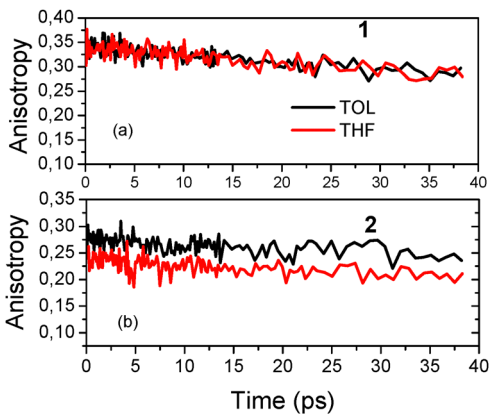

Fig. 6 Anisotropy dynamics within the first 40 ps measured by the up-conversion technique for **1** (a) and **2** (b) in TOL and THF.

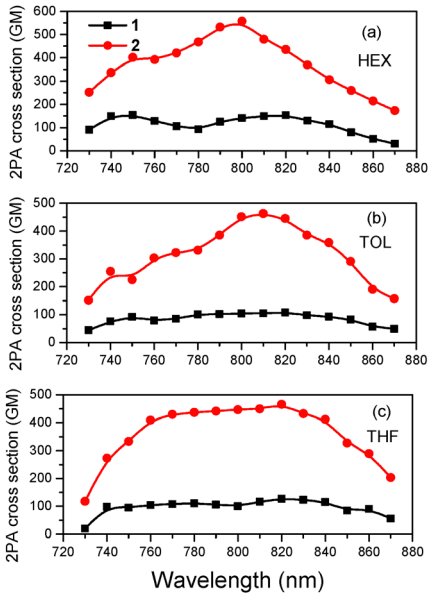

Fig. 7 2PA spectra of **1** and **2** in (a) HEX, (b) TOL and (c) THF.

Two-photon absorption properties

The 2PA spectra are presented in Fig. 7 for both molecules in HEX, TOL and THF. The two-photon induced fluorescence as a function of excitation intensity is shown in Fig. S12 (ESI†) exhibiting the quadratic dependence as expected for a 2PA process. Due to its longer conjugation length, **2** has larger 2PA cross sections than its dipolar counterpart reaching 560 GM in HEX and 450 GM in TOL and THF. Apart from the difference in the 2PA values, the 2PA peak of **2** falls within the same spectral region as that of **1**, meaning that the spectral shift observed in their 1PA spectra is not maintained. 2PA spectroscopy is, in general, useful in identifying the nature and molecular geometry of the excited states.[110] A comparison of 2PA spectra with the rescaled 1PA ones is shown in Fig. S13 (ESI†). For **2**, the 2PA peak is blue-shifted compared to twice the wavelength of the rescaled 1PA peak, following the expected behavior of a quadrupolar molecule based on the Frenkel exciton model.[33,87,111] Besides, the 2PA and rescaled 1PA spectra of **1** coincide, providing further evidence for its dipolar behavior as also concluded by the fs-anisotropy measurements. However, even in non-centrosymmetric chromophores, a blue-shift of the 2PA band relative to the 1PA one can be observed due to an involvement of enhanced vibronic transitions in the 2PA spectrum.[112]

Mono- and di(diphenylamino)styrylpyrimidines have been extensively studied in the past for their 2PA properties.[76] In this frame, the effects of the electron donating group, branching and π-conjugated bridge have been addressed.[113–115] Surprisingly, very large 2PA cross section values reaching 3000 GM have been found. However, great care must be taken when discussing and comparing different results since in certain cases very high excitation powers and sample concentrations have been used. On the other hand, a comparison of the 2PA values of **1** and **2** can be made with those of the molecules presented in our previous work,[50] where the acridan group is replaced by another diphenylamino substituent, addressing the influence of the C2 substitution. Interestingly, the three-branched A–(π–D)$_3$ compound with diphenylamino groups at the periphery (2c in ref. 50) has very similar 2PA cross section values and peak wavelengths compared to **2**, showing that the replacement of the diphenylamino with the out-of-plane oriented acridan does not play a decisive role in the 2PA properties.

Finally, the 2PA results are also useful in calculating again the difference between the excited and ground state dipole moments using the equation:[19,116,117]

$$\Delta\mu_{2PA} = \left(\frac{5}{4(1+2\cos^2\theta)} \frac{hcN_A}{\pi 10^3 \ln 10} \frac{n}{f_{opt}^2} \frac{\nu_{max}}{\varepsilon_{max}} \delta_{2PA}(0-0) \right)^{1/2}$$

where ν_{max} is the lowest energy absorption frequency (in Hz), ε_{max} is the peak molar absorption coefficient (in mol^{-1} dm^3 cm^{-1}), θ is the angle between the dipole moments of the excited and ground states (considered as $\theta = 0$), n is the refractive index and f_{opt} is the local field factor equal to $(2 + n^2)/3$. The difference in the permanent dipole moments of the ground and excited states was calculated and compared with those found from the solvation method. $\Delta\mu_{2PA}$ in TOL was found to be 12.9 and 17.00 D for **1** and **2**, respectively, which are in reasonable agreement with those found using the Lippert–Mataga plots (Table S3, ESI†).

Conclusions

In summary, we have investigated the role of branching in the steady-state, excited state dynamics and 2PA properties of two pyrimidine molecules with a phenylacridan group at the C2 position. The pyrimidine was also substituted at the C4/6 positions with styryl groups attached to diphenylamino donors to obtain molecules **1** and **2**. Steady state spectroscopy shows a larger Stokes shift for molecule **1**, while higher fluorescence quantum yields were obtained for **2**. The time-resolved fluorescence measurements revealed emission pathways attributed to a FC-CT and a R-CT state. For **1** in THF, the R-CT population occurs as fast as inertial solvation, followed by diffusive solvation of the R-CT state. On the other hand, for **2**, the FC-CT to R-CT energy transfer is slower than that for **1**, occurring by the solvated FC-CT state. Time resolved anisotropy measurements in the fs–ps timescale showed an excited state of dipolar and pseudo-quadrupolar nature for **1** and **2**, respectively. Finally, 2PA characterization showed a more than 4 times increase of the 2PA cross sections for **2** *vs.* **1**, reaching 560 GM at 820 nm in HEX.

Author contributions

Investigation: AK, MFec, MF; methodology: MF; writing – original draft: MF; writing – review and editing: MF, SA and FB.

Data availability

The data supporting this article are available upon request.

Conflicts of interest

There are no conflicts to declare.

Acknowledgements

Part of this work was supported by the ERDF "Innovative materials suitable for high added value applications (INMA)" (No. CZ.02.01.01/00/23_021/0008593). M. F. acknowledges the Région Bretagne, France, for her PhD funding (HOLED project).

References

1 P. K. Samanta and R. Misra, *J. Appl. Phys.*, 2023, **133**, 020901.
2 F. Bureš, *RSC Adv.*, 2014, **4**, 58826.
3 H. Miranda-Salinas, Y.-T. Hung, Y.-S. Chen, D. Luo, H.-C. Kao, C.-H. Chang, K.-T. Wong and A. Monkman, *J. Mater. Chem. C*, 2021, **9**, 8819.
4 C. Zhu, T. Wei, Y. Wei, L. Wang, M. Lu, Y. Yuan, L. Yin and L. Huang, *J. Mater. Chem. A*, 2021, **9**, 1207.
5 Z. Zhao, C. Zeng, X. Peng, Y. Liu, H. Zhao, L. Hua, S.-J. Su, S. Yan and Z. Ren, *Angew. Chem., Int. Ed.*, 2022, **61**, e202210864.
6 C. S. Abeywickrama, *Chem. Commun.*, 2022, **58**, 9855.
7 N. Yukihira, C. Uragami, K. Horiuchi, D. Kosumi, A. T. Gardiner, R. J. Cogdell and H. Hashimoto, *Commun. Chem.*, 2022, **5**, 135.
8 Y.-X. Tan, X. Zhang, Y. Wang and J. Yao, *Acc. Mater. Res.*, 2024, **5**, 1377.
9 A. M. Gutiérrez-Vílchez, C. V. Ileperuma, V. Navarro-Pérez, P. A. Karr, F. Fernández-Lázaro and F. D'Souza, *ChemPlusChem*, 2024, **89**, e202400348.
10 C. Qin, X. Wu, L. Tang, X. Chen, M. Li, Y. Mou, B. Su, S. Wang, C. Feng, J. Liu, X. Yuan, Y. Zhao and H. Wang, *Nat. Commun.*, 2023, **14**, 5238.
11 Y. Rout, C. Montanari, E. Pasciucco, R. Misra and B. Carlotti, *J. Am. Chem. Soc.*, 2021, **143**, 9933.
12 V. Maffeis, R. Brisse, V. Labet, B. Jousselme and T. Gustavsson, *J. Phys. Chem. A*, 2018, **122**, 5533.
13 D. Fan, Y. Yi, Z. Li, W. Liu, Q. Peng and Z. Shuai, *J. Phys. Chem. A*, 2015, **119**, 5233.
14 Y. Hu, C. Neumann, L. Scholtz, A. Turchanin, U. Resch-Genger and S. Eigler, *Nano Res.*, 2023, **16**, 45.
15 F. Barati-Darband, M. Izadyar and F. Arkan, *J. Phys. Chem. A*, 2019, **123**, 2831.
16 Y. Li, M. Zhou, Y. Niu, Q. Guo and A. Xia, *J. Chem. Phys.*, 2015, **143**, 034309.
17 Y. Zhang, M. Jiang, G.-C. Han, K. Zhao, B. Z. Tang and K. S. Wong, *J. Phys. Chem. C*, 2015, **119**, 27630.
18 D. J. Stewart, M. J. Dalton, R. N. Swiger, J. L. Fore, M. A. Walker, T. M. Cooper, J. E. Haley and L.-S. Tan, *J. Phys. Chem. A*, 2014, **118**, 5228.
19 B. Carlotti, E. Benassi, C. G. Fortuna, V. Barone, A. Spalletti and F. Elisei, *Chem. Phys. Chem.*, 2016, **17**, 136.
20 B. Carlotti, E. Benassi, A. Spalletti, C. G. Fortuna, F. Eliseia and V. Barone, *Phys. Chem. Chem. Phys.*, 2014, **16**, 13984.
21 F. Xiao, X. Liu, K. Lin, Y. Zhou, W. Gao, Y. Lei, M. Liu, X. Huang and H. Wu, *J. Phys. Chem. C*, 2021, **125**, 16792.
22 S. Sasaki, G. P. C. Drummen and G. Konishiac, *J. Mater. Chem. C*, 2016, **4**, 2731.
23 S. Kumar, P. Singh, P. Kumar, R. Srivastava, S. Kalyan Pal and S. Ghosh, *J. Phys. Chem. C*, 2016, **120**, 12723.
24 H.-Y. Fu, X.-J. Liu, H. Zha, X.-X. Li, Y. Xu, F. Yanga and M. Xia, *Phys. Chem. Chem. Phys.*, 2019, **21**, 1399.
25 K. Hanaoka, S. Iwaki, K. Yagi, T. Myochin, T. Ikeno, H. Ohno, E. Sasaki, T. Komatsu, T. Ueno, M. Uchigashima, T. Mikuni, K. Tainaka, S. Tahara, S. Takeuchi, T. Tahara, M. Uchiyama, T. Nagano and Y. Urano, *J. Am. Chem. Soc.*, 2022, **144**, 19778.
26 R. Ghosh, *Phys. Chem. Chem. Phys.*, 2018, **20**, 6347.
27 D.-G. Chen, T.-C. Lin, Y.-A. Chen, Y.-H. Chen, T.-C. Lin, Y.-T. Chen and P.-T. Chou, *J. Phys. Chem. C*, 2018, **122**, 12215.
28 L. Martinez-Fernandez, T. Gustavsson, U. Diederichsen and R. Improta, *Molecules*, 2020, **25**, 824.
29 P. K. Singh, S. Nath, M. Kumbhakar, A. C. Bhasikuttan and H. Pal, *J. Phys. Chem. A*, 2008, **112**, 5598.
30 J. Sung, P. Kim, Y. O. Lee, J. S. Kim and D. Kim, *J. Phys. Chem. Lett.*, 2011, **2**, 818.
31 B. Dereka, A. Rosspeintner, Z. Li, R. Liska and E. Vauthey, *J. Am. Chem. Soc.*, 2016, **138**, 4643.
32 B. Dereka, A. Rosspeintner, R. Stężycki, C. Ruckebusch, D. T. Gryko and E. Vauthey, *J. Phys. Chem. Lett.*, 2017, **8**, 6029.
33 F. Terenziani, A. Painelli, C. Katan, M. Charlot and M. Blanchard-Desce, *J. Am. Chem. Soc.*, 2006, **128**, 15742.
34 M. Fakis, V. Petropoulos, P. Hrobárik, J. Nociarová, P. Osuský, M. Maiuri and G. Cerullo, *J. Phys. Chem. B*, 2022, **126**, 8532.
35 J. Kong, W. Zhang, G. Li, D. Huo, Y. Guo, X. Niu, Y. Wan, B. Tang and A. Xia, *J. Phys. Chem. Lett.*, 2020, **11**, 10329.
36 R. Roy, S. Chawla, V. Sharma, A. K. Pal, Y. Silori, A. Datta, A. K. De and A. Lal Koner, *Chem. Sci.*, 2024, **15**, 6363–6377.
37 A. Cesaretti, A. Spalletti, F. Elisei, P. Foggi, R. Germani, C. G. Fortuna and B. Carlotti, *Phys. Chem. Chem. Phys.*, 2021, **23**, 16739.
38 J. Wu, W. Wang, C. Gong, Q. Li, Z. Li, G. Deng, X. Zhang, K. Chen, Y. Gong and K. S. Chiangac, *J. Mater. Chem. C*, 2017, **5**, 7472.
39 K. Senthilkumar, M. Pizzotti, K. Thirumoorthy, G. Di Carlo, S. Righetto, A. O. Biroli, M. Haukka and N. Palanisami, *J. Phys. Chem. C*, 2016, **120**, 20277.
40 J. M. Cole, *R. Soc. A*, 2003, **361**, 2751.
41 Y. Peng, Y. Yan, P. Li, B. Li, H. Jiang, B. Guo, Q. Yuan and W. Gan, *Mater. Chem. Front.*, 2023, **7**, 502.
42 L. Sun, W. Zhu, W. Wang, F. Yang, C. Zhang, S. Wang, X. Zhang, R. Li, H. Dong and W. Hu, *Angew. Chem.*, 2017, **56**, 7831.
43 S. Sarkar, M. Santra, S. Singha, Y. W. Jun, Y. J. Reo, H. R. Kima and K. H. Ahn, *J. Mater. Chem. B*, 2018, **6**, 4446.
44 S. Pascal, Q. Bellier, S. David, P.-A. Bouit, S.-H. Chi, N. S. Makarov, B. Le Guennic, S. Chibani, G. Berginc,

P. Feneyrou, D. Jacquemin, J. W. Perry, O. Maury and C. Andraud, *J. Phys. Chem. C*, 2019, **123**, 23661.
45 L. Lescos, P. Beaujean, C. Tonnelé, P. Aurel, M. Blanchard-Desce, V. Rodriguez, M. de Wergifosse, B. Champagne, L. Muccioli and F. Castet, *Phys. Chem. Chem. Phys.*, 2021, **23**, 23643.
46 F. Terenziani, C. Katan, E. Badaeva, S. Tretiak and M. Blanchard-Desce, *Adv. Mater.*, 2008, **20**, 4641.
47 M. G. Vivas, D. L. Silva, J. Malinge, M. Boujtita, R. Zaleśny, W. Bartkowiak, H. Ågren, S. Canuto, L. De Boni, E. Ishow and C. R. Mendonca, *Sci. Rep.*, 2014, **4**, 4447.
48 J. Nociarová, P. Osuský, E. Rakovský, D. Georgiou, I. Polyzos, M. Fakis and P. Hrobárik, *Org. Lett.*, 2021, **23**, 3460.
49 P. Osusky, J. Nociarova, M. Smolicek, R. Gyepes, D. Georgiou, I. Polyzos, M. Fakis and P. Hrobarik, *Org. Lett.*, 2021, **23**, 5512.
50 F. Kournoutas, A. Fihey, J.-P. Malval, A. Spangenberg, M. Fecková, P. le Poul, C. Katan, F. Robin-le Guen, F. Bureš, S. Achelle and M. Fakis, *Phys. Chem. Chem. Phys.*, 2020, **22**, 4165.
51 D. Kim, H. Moon, S. H. Baik, S. Singha, Y. W. Jun, T. Wang, K. H. Kim, B. S. Park, J. Jung, I. Mook-Jung and K. H. Ahn, *J. Am. Chem. Soc.*, 2015, **137**, 6781.
52 Y. Shen, A. J. Shuhendler, D. Ye, J.-J. Xua and H.-Y. Chen, *Chem. Soc. Rev.*, 2016, **45**, 6725.
53 Y. Morel, A. Irimia, P. Najechalski, Y. Kervella, O. Stephan, P. L. Baldeck and C. Andraud, *J. Chem. Phys.*, 2001, **114**, 5391.
54 Q. Zheng, S. K. Gupta, G. S. He, L.-S. Tan and P. N. Prasad, *Adv. Funct. Mater.*, 2008, **18**, 2770.
55 G. Williams, M. Hunt, B. Boehm, A. May, M. Taverne, D. Ho, S. Giblin, D. Read, J. Rarity, R. Allenspach and S. Ladak, *Nano Res.*, 2018, **11**, 845.
56 Q. Geng, D. Wang, P. Chen and S.-C. Chen, *Nat. Commun.*, 2019, **10**, 2179.
57 M. Gu, Q. Zhang and S. Lamon, *Nat. Rev. Mater.*, 2016, **1**, 16070.
58 J. M. Dos Santos, D. Hall, B. Basumatary, M. Bryden, D. Chen, P. Choudhary, T. Comerford, E. Crovini, A. Danos, J. De, S. Diesing, M. Fatahi, M. Griffin, A. K. Gupta, H. Hafeez, L. Hämmerling, E. Hanover, J. Haug, T. Heil, D. Karthik, S. Kumar, O. Lee, H. Li, F. Lucas, C. F. R. Mackenzie, A. Mariko, T. Matulaitis, F. Millward, Y. Olivier, Q. Qi, I. D. W. Samuel, N. Sharma, C. Si, L. Spierling, P. Sudhakar, D. Sun, E. Tankelevičiūtė, M. D. Tonet, J. Wang, T. Wang, S. Wu, Y. Xu, L. Zhang and E. Zysman-Colman, *Chem. Rev.*, 2024, **124**, 13736.
59 Z. Yang, Z. Mao, Z. Xie, Y. Zhang, S. Liu, J. Zhao, J. Xu, Z. Chi and M. P. Aldred, *Chem. Soc. Rev.*, 2017, **46**, 915.
60 Y. Tao, K. Yuan, T. Chen, P. Xu, H. Li, R. Chen, C. Zheng, L. Zhang and W. Huang, *Adv. Mater.*, 2014, **26**, 7931.
61 M. Y. Wong and E. Zysman-Colman, *Adv. Mater.*, 2017, **29**, 1605444.
62 Y. Shimomura and G. Konishi, *Chem. – Eur. J.*, 2023, **29**, e202301191.
63 M. Mahato, T. Sultana, R. Sahoo, S. Ahamed, N. Tohora, A. Maitia and S. K. Das, *Phys. Chem. Chem. Phys.*, 2025, **27**, 1366.
64 Z. Kang, S.-C. Chen, Y. Ma, J. Wang and Q. Zheng, *ACS Appl. Mater. Interfaces*, 2017, **9**, 24771.
65 A. A. Raheem, S. Kamaraj, V. Sannasi and C. Praveen, *Org. Chem. Front.*, 2018, **5**, 777.
66 N. Altinolcek, A. Battal, C. Nur Vardalli, M. Tavasli, H. A. Yu, W. J. Peveler and P. J. Skabara, *J. Mol. Struct.*, 2021, **1239**, 130494.
67 G. Tang, W. Yang and J. Zhao, *J. Phys. Chem. A*, 2022, **126**, 3653.
68 A. Karatay, H. Yılmaz, E. A. Yildiz, G. Sevinç, M. Hayvali, B. Boyacioglu, H. Unvere and A. Elmalia, *Phys. Chem. Chem. Phys.*, 2022, **24**, 25495.
69 D. Cvejn, E. Michail, K. Seintis, M. Klikar, O. Pytela, T. Mikysek, N. Almonasy, M. Ludwig, V. Giannetas, M. Fakis and F. Bureš, *RSC Adv.*, 2016, **6**, 12819.
70 Y. Gong, G.-L. Hou, X. Bi, N. Kuthirummal, A. A. Teklu, J. Koenemann, N. Harris, P. Wei, K. Devera and M. Hu, *J. Phys. Chem. A*, 2021, **125**, 1870.
71 X. Liang, B. Dong, H. Wang, Z. Zhang, S. Wang, J. Li, B. Zhao, Z. Li, Y. Xinga and K. Guo, *J. Mater. Chem. C*, 2022, **10**, 7857.
72 B. K. Kundu, G. Han and Y. Sun, *J. Am. Chem. Soc.*, 2023, **145**, 3535.
73 D. J. Stewart, R. Kannan, T. A. Grusenmeyer, J. M. Artz, S. L. Long, Z. Yu, T. M. Cooper, J. E. Haleya and L.-S. Tan, *Phys. Chem. Chem. Phys.*, 2018, **20**, 19398.
74 P. Šimon, M. Klikar, Z. Burešová, C. Vourdaki, A. Katsidas, J. Tydlitát, J. Kulhánek, J. Zelenka, M. Fakis and F. Bureš, *J. Mater. Chem. C*, 2023, **11**, 7252.
75 M. Tromayer, P. Gruber, A. Rosspeintner, A. Ajami, W. Husinsky, F. Plasser, L. González, E. Vauthey, A. Ovsianikov and R. Liska, *Sci. Rep.*, 2018, **8**, 17273.
76 M. Fecková, P. le Poul, F. Bureš, F. Robin-le Guen and S. Achelle, *Dyes Pigm.*, 2020, **182**, 108659.
77 S. Achelle, M. Hodée, J. Massue, A. Fihey and C. Katan, *Dyes Pigm.*, 2022, **200**, 110157.
78 S. Achelle, J. Rodríguez-López, F. Bureš and F. Robin-le Guen, *Chem. Rec.*, 2020, **20**, 440.
79 S. Achelle, J. Rodríguez-López and F. Robin-le Guen, *Org. Biomol. Chem.*, 2023, **21**, 39.
80 M. Fecková, I. K. Kalis, T. Roisnel, P. le Poul, O. Pytela, M. Klikar, F. Robin-le Guen, F. Bureš, M. Fakis and S. Achelle, *Chem. Eur. J.*, 2021, **27**, 1145.
81 M. Taniguchi and J. S. Lindsey, *Photochem. Photobiol.*, 2018, **94**, 290.
82 V. Petropoulos, I. Georgoulis, C. Vourdaki, P. Hrobárik, I. Sigmundová, J. Nociarová, M. Maiuri, G. Cerullo and M. Fakis, *Chem. Phys. Chem.*, 2023, **24**, e202300127.
83 P. Hrobarik, V. Hrobarikova, I. Sigmundova, P. Zahradnik, M. Fakis, I. Polyzos and P. Persephonis, *J. Org. Chem.*, 2011, **76**, 8726.
84 N. S. Makarov, M. Drobizhev and A. Rebane, *Opt. Express.*, 2008, **16**, 4029.
85 S. de Reguardati, J. Pahapill, A. Mikhailov, Y. Stepanenko and A. Rebane, *Opt. Express.*, 2016, **24**, 9053.
86 U. Subuddhi, S. Haldar, S. Sankararaman and A. K. Mishra, *Photochem. Photobiol. Sci.*, 2006, **5**, 459.

87 P. Suppan, *J. Photochem. Photobiol., A*, 1990, **50**, 293.
88 C. Katan, F. Terenziani, O. Mongin, M. H. V. Werts, L. T. Porrès, T. Pons, J. Mertz, S. Tretiak and M. Blanchard-Desce, *J. Phys. Chem. A*, 2005, **109**, 3024.
89 L. Yan, X. Chen, Q. He, Y. Wang, X. Wang, Q. Guo, F. Bai, A. Xia, D. Aumiler, S. Vdović and S. H. Lin, *J. Phys. Chem. A*, 2012, **116**, 8693.
90 F. Terenziani, C. LeDroumaguet, C. Katan, O. Mongin and M. Blanchard-Desce, *Chem. Phys. Chem.*, 2007, **8**, 723.
91 J. E. Lewis and M. Maroncelli, *Chem. Phys. Lett.*, 1998, **282**, 197.
92 S. J. Strickler and R. A. Berg, *J. Chem. Phys.*, 1962, **37**, 814.
93 M. I. Sluch, A. Godt, U. H. F. Bunz and M. A. Berg, *J. Am. Chem. Soc.*, 2001, **123**, 6447.
94 B. Dereka, A. Rosspeintner, R. Stężycki, C. Ruckebusch, D. T. Gryko and E. Vauthey, *J. Phys. Chem. Lett.*, 2017, **8**, 6029.
95 J. R. Lacowicz, *Principles of Fluorescence Spectroscopy*, Springer, 2006.
96 M. Jia, X. Ma, L. Yan, H. Wang, Q. Guo, X. Wang, Y. Wang, X. Zhan and A. Xia, *J. Phys. Chem. A*, 2010, **114**, 7345.
97 M. Eugenio Vazquez, J. B. Blanco and B. Imperiali, *J. Am. Chem. Soc.*, 2005, **127**, 1300–1306.
98 N. Periasamy and A. S. R. Koti, *Proc. Indian Natn. Sci. Acad.*, 2003, **69**, A41.
99 P. K. Singh, M. Kumbhakar, H. Pal and S. Nath, *J. Phys. Chem. B*, 2010, **114**, 5920.
100 A. K. Mora and S. Nath, *J. Phys. Chem. B*, 2019, **123**, 8767.
101 S. R. Rather and P. Sen, *J. Chem. Phys.*, 2013, **138**, 084308.
102 S. Santra, A. K. Mora and S. Nath, *J. Photochem. Photobiol., A*, 2023, **437**, 114474.
103 M. L. Horng, J. A. Gardecki, A. Papazyan and M. Maroncelli, *J. Phys. Chem.*, 1995, **99**, 17311.
104 L. Reynolds, J. A. Gardecki, S. J. V. Frankland, M. L. Horng and M. Maroncelli, *J. Phys. Chem.*, 1996, **100**, 10337.
105 J. S. Beckwith, A. Rosspeintner, G. Licari, M. Lunzer, B. Holzer, J. Fröhlich and E. Vauthey, *J. Phys. Chem. Lett.*, 2017, **8**, 5878.
106 X. Niu, Z. Kuang, M. Planells, Y. Guo, N. Robertson and A. Xia, *Phys. Chem. Chem. Phys.*, 2020, **22**, 15743.
107 N. A. Montgomery, G. J. Hedley, A. Ruseckas, J. C. Denis, S. Schumacher, A. L. Kanibolotsky, P. J. Skabara, I. Galbraith, G. A. Turnbull and I. D. W. Samuel, *Phys. Chem. Chem. Phys.*, 2012, **14**, 9176–9184.
108 O. P. Varnavski, J. C. Ostrowski, L. Sukhomlinova, R. J. Twieg, G. C. Bazan and T. Goodson III, *J. Am. Chem. Soc.*, 2002, **124**, 1736–1743.
109 K. Seintis, D. Agathangelou, D. Cvejn, N. Almonasy, F. Bureš, V. Giannetas and M. Fakis, *Phys. Chem. Chem. Phys.*, 2017, **19**, 16485–16497.
110 N. S. Makarov, S. Mukhopadhyay, K. Yesudas, J.-L. Brédas, J. W. Perry, A. Pron, M. Kivala and K. Müllen, *J. Phys. Chem. A*, 2012, **116**, 3781.
111 C. Sissa, V. Parthasarathy, D. Drouin-Kucma, M. H. V. Werts, M. Blanchard-Desce and F. Terenziani, *Phys. Chem. Chem. Phys.*, 2010, **12**, 11715.
112 M. Drobizhev, N. S. Makarov, S. E. Tillo, T. E. Hughes and A. Rebane, *Nat. Methods*, 2011, **8**, 393.
113 L. Li, Y.-P. Tian, J.-X. Yang, P.-P. Sun, J.-Y. Wu, H.-P. Zhou, S.-Y. Zhang, B.-K. Jin, X.-J. Xing, C.-K. Wang, M. Li, G.-H. Cheng, H.-H. Tang, W.-H. Huang, X.-T. Tao and M.-H. Jiang, *Chem. – Asian J.*, 2009, **4**, 668.
114 B. Liu, X.-L. Hu, J. Liu, Y.-D. Zhao and Z.-L. Huang, *Tetrahedron Lett.*, 2007, **48**, 5958.
115 Q. Zhang, L. Luo, H. Xu, Z. Hu, C. Brommesson, J. Wu, Z. Sun, Y. Tian and K. Uvdal, *New J. Chem.*, 2016, **40**, 3456.
116 A. Rebane, M. Drobizhev, N. S. Makarov, G. Wicks, P. Wnuk, Y. Stepanenko, J. E. Haley, D. M. Krein, J. L. Fore, A. R. Burke, J. E. Slagle, D. G. McLean and T. M. Cooper, *J. Phys. Chem. A*, 2014, **118**, 3749.
117 A. Rebane, M. Drobizhev, N. S. Makarov, E. Beuerman, J. E. Haley, D. M. Krein, A. R. Burke, J. L. Flikkema and T. M. Cooper, *J. Phys. Chem. A*, 2011, **115**, 4255.

